HP-LT metamorphism in Elba Island: Implications for the geodynamic evolution of the inner Northern Apennines (Italy)

HP-LT metamorphism in Elba Island: implications for the geodynamic evolution of inner Northern Apennines (Italy)

Caterina Bianco*+, Andrea Brogi*, Alfredo Caggianelli*,
Giovanna Giorgetti**, Domenico Liotta*, Marco Meccheri**

* *Dipartimento di Scienze della Terra e Geoambientali, Via Orabona 4, Bari, Italy*

** *Dipartimento di Scienze Fisiche, della Terra, ed Ambientali, Via Laterina 4, Siena, Italy*

+corresponding Author: caterina.bianco@uniba.it

Abstract

The inner Northern Apennines (*i.e.,* northern Tyrrhenian Sea and southern Tuscany) is an Alpine chain affected by high-P metamorphic condition during its evolution. Although the Elba Island is structurally located close to the Adria-Europe suture zone, no evidence of high-P metamorphism has been here documented. This led to consider it as a sector of the orogeny developed in a low P-context. This paper accounts for a new finding of high-P and low-T metamorphism documented in metabasite rocks embedded in the Cretaceous calcschist of eastern Elba Island. Mineral composition of metabasite includes Gln+Cpx+Ep+Ab+Act+Qtz+Ilm±Ti-oxide±Spn and it is indicative of a former equilibration in the epidote blueschist subfacies and subsequent retrogression in the greenschist facies. Metamorphic peak occurred at P= 0.9-1.0 GPa and T=330-350°C. Tectonic discrimination using immobile elements in the metabasite does not point to an oceanic setting. As a consequence, the metasedimentary succession containing metabasite is interpreted as belonging to the Tuscan contintental domain and not to the Ligurian-Piedmont Ocean, as previously interpreted. Our results have two significant implications: (i) the tectonic stacking of the Elba Island units did not occur in a low-pressure context; (ii) the Elba Island is now reconciled in the tectonic and metamorphic evolution of the inner Northern Apennines.

1. **Introduction**

Northern Apennines is an eastward verging alpine belt deriving from the convergence and subsequent collision between Adria microplate and Corsica-Sardinia massif, believed of African and European pertinence, respectively (Molli, 2008 with references therein).

Evidence of high-P metamorphic conditions have been detected, both in metasiliciclastic rocks and metabasite, along a roughly W-E transect, from the Tuscan Archipelago up to the exhumed Metamorphic Complex cropping out in southern Tuscany (Fig.1).

Data from metasediments indicate P-T values (Fig.1) of 1.0-1.5 GPa and $\leq$ 350 °C, in the Tuscan Archipelago (Rossetti et al., 1999; Rossetti et al., 2001). Differently, inland, the P-values are slightly lower, between 0.6 – 1.2 GPa and T is in the range 350–420 °C (Kligfield et al., 1986; Theye et al., 1997; Giorgetti et al., 1998; Elter and Pandeli, 2002; Brogi and Giorgetti, 2012). High-P metamorphism is dated at Late Oligocene-Early Miocene, on the basis of $^{40}Ar/^{39}Ar$ radiometric method (Brunet et al. 2000).

Higher and older thermobaric conditions are recorded in north-eastern Corsica where P-T values up to 2 GPa and 380°C have been detected and referred to Eocene (Jolivet et al., 1998; Brunet et al., 2000) and Oligocene (Rossetti et al., 2015). These data are associated to westward verging thrusts (Fig.1) involving the oceanic rocks presently exposed in the Alpine Corsica.

Thus, along the Corsica-Tuscany W-E transect (Fig.1), the Elba Island represents the westernmost outcropping evidence of tectonic units verging to the east (Trevisan, 1950), as it is the case of the Apennine belt. In addition, and as further on described, the structure of the Elba Island is characterised by the superimposition of continental units over the oceanic ones, the latter already stacked on the continental successions (Pertusati et al., 1993 with references).

This fact, therefore, enforced the interpretation that the collisional suture between the European and African plates passes close to the Elba Island (Keller and Pialli, 1990; Pandeli et al., 2001; Balestrieri et al., 2011). However, although studies on Si-content in phengite suggested high-P occurrence (Pandeli et al., 2001), the lack of a mineral assemblage confirming high-P and low-T metamorphic conditions, makes this interpretation weak, thus accounting for orogenic (Late Oligocene-Early Miocene) deformation developed under low-P metamorphic conditions (Keller and Coward, 1996; Garfagnoli et al., 2005; Musumeci and Vaselli, 2012). For this reason, Elba Island resulted a distinctive case with respect to the surrounding areas, with fallouts on the supposed evolution of the Northern Tyrrhenian Basin (Bonini et al., 2014).

In this paper we document for the first time, the occurrence of a high-P mineral assemblage in metabasite interlayered to Cretaceous calcschist (Acquadolce Unit *Auctt*.). We conclude that high-P and low-T metamorphism affected the whole tectonic pile of the Elba Island, at least up to the Early Burdigalian, as suggested by Deino et al. (1992) age measurements, thus reconciling the evolution of the Elba Island with the Northern Apennines.

2. Geological framework

The geodynamic process leading to the Northern Apennines orogenesis determined the eastward stacking of several tectonic units belonging to oceanic and continental paleogeographic domains. These are: (*a*) the Ligurian Units, consisting of remnants of Jurassic oceanic crust, with the Jurassic-Cretaceous cover (Ligurian Units) and Cretaceous-Oligocene turbidites (Sub-Ligurian Units); these units were thrust eastwards over the Tuscan Nappe during Late Oligocene-Early Miocene times; (*b*) the inner Tuscan Domain, made up of a complete sedimentary succession of evaporitic, platform, pelagic and foredeep environments, ranging in age from Late Trias to Early Miocene. During Early Miocene, the Tuscan succession was internally deformed and detached from its substratum along the late Triassic evaporite level, giving rise to the Tuscan Nappe. This latter stacked over the external Tuscan domain, that was deformed in isoclinal folds and duplex structures, under metamorphic conditions from the blueschist to the greenschist facies (Carmignani and Kligfield, 1990; Carmignani et al., 1994; Jolivet et al., 1998; Rossetti et al., 2002; Molli, 2008; Brunet et al., 2000; Brogi and Giorgetti, 2012). During Early-Middle Miocene (Jolivet et al., 1990; Carmignani et al., 1995; Brunet et al., 2000) the tectonic framework changed and an eastward migrating extension affected the inner Northern Apennines (i.e., northern Tyrrhenian Sea and southern Tuscany). Extension continuously developed through time, although two main events can be distinguished (Barchi, 2010 with references therein). The first one, occurred during Miocene, determined the lateral segmentation of the more competent levels within the previously stacked tectonic units and the consequent superimposition of the Ligurian Units (at the top of the tectonic pile) on the deeper basal detachment levels. These are within the late Triassic evaporite and the Palaeozoic phyllite (Bertini et al., 1991; Baldi et al., 1994), and, consequently, the stair-case geometry of the faults gave rise to bowl-shaped structural depressions where Langhian-Messinian marine to evaporitic and continental sediments deposited (Brogi and Liotta, 2008). The second extensional event (Pliocene-Quaternary) determined normal faults crosscutting the previously developed compressional and extensional structures, thus defining tectonic depressions filled up by Pliocene to Quaternary marine and continental sediments (Bossio et al., 1993). Since Late Miocene, extension is accompanied by anatectic magmatism with minor mantle contribution (Peccerillo, 2003).

2.1. Elba Island geological framework

Integrating previous papers (Trevisan, 1950; Keller and Pialli, 1990; Pertusati et al., 1993; Bortolotti et al., 2001 with references therein) with the data here further on illustrated, we distinguish seven main tectonic units, belonging both to continental and oceanic environments and forming the tectonic pile of the Elba Island (Fig.2). The deeper outcropping continental unit (continental unit 1, Fig.3) is made up of early Carboniferous micaschist (Musumeci et al., 2011) and its Triassic-Jurassic siliciclastic and carbonatic cover (Porto Azzurro Unit, in Pandeli et al., 2005).

The 2nd continental unit (Fig.3) is made up of a complete succession of metamorphic rocks consisting of middle Ordovician porphyroids (Ortano porphyroids, Musumeci et al., 2011) above which Mesozoic continental to marine metasediments crop out (Duranti et al., 1992). The latter are late Triassic to Jurassic metacarbonates, calcschist and metaradiolarite passing to a Cretaceous succession made up of calcschist and phyllite with levels of metasiltstone and metasandstone. Calcschist represents the base of the succession and contains discontinuous lenses of metabasite (Fig.3), the main focus of this paper. The third continental unit (Fig.3) consists of low-grade metamorphic rocks including late Carboniferous phyllite, overlain by Triassic continental quartzite and phyllite, marine ?Triassic-?Jurassic marble and by the

Cretaceous-Oligocene carbonatic and terrigenous metasedimentary succession (Bortolotti et al., 2001). Finally, the forth continental unit (Fig.3) is related to the Tuscan Nappe, composed of late Triassic, locally vacuolar and fragmented calcareous dolostone, overlain by Jurassic marine carbonate and Cretaceous-Oligocene calcareous and marly pelagic sediments. The oceanic unit 1 (Fig.3) is interposed between the second and the third continental units by means of out-of-sequence thrust (Keller and Pialli, 1990; Pertusati et al., 1993; Keller and Coward, 1996) referred to Early Burdigalian (Deino et al., 1992; Pertusati et al., 1993). This unit is a tectonic slice made up of Jurassic ophiolite. Finally, the oceanic units 2 and 3 (Fig.3) consist of remnants of the Jurassic ophiolite, Jurassic radiolarite and Cretaceous-Eocene calcareous and terrigenous sediments, with levels of ophiolitic breccias. After the stacking of the tectonic pile, the Elba Island was affected by Miocene extensional structures and magmatism (Fig.2), giving rise to the emplacement of Monte Capanne (about 7.0 Ma, Westerman et al., 2004), and Porto Azzurro (about 6 Ma, Maineri et al. 2003 and Musumeci et al. 2011) laccolith-pluton-dyke granitic complexes (Dini et al. 2002), respectively located to the West and East sides of the Island (Fig.2). Regionally, magma emplacement and cooling (Caggianelli et al., 2014) determined thermo-metamorphic aureolas (Barberi and Innocenti, 1965; Duranti et al., 1992; Rossetti et al., 2007) and low-P mineral assemblage resetting the older metamorphic paragenesis related to the collisional event (Duranti et al., 1992; Pertusati et al., 1993). Moreover, a diffuse hydrothermalism determined Fe-ore deposits (Tanelli, 1983; Tanelli et al., 2001), particularly in the Eastern Elba Island. In this framework, it was surprising to find relic high-pressure metamorphic paragenesis still preserved in metabasite lithons, embedded in the calcshist of the Continental unit 2 (Fig.3).

3 - Rock fabric

The sampling area (Fig.4 and Fig. 5A) is structurally located in the lower part of the Cretaceous succession of the continental unit 2 (Fig.3). Here, lenses of metabasite, from few cm to about 2 m thick (Fig. 5B), are embedded in calcschist, mainly along the main schistosity, gently NW-dipping (Fig.5C-5D). The metabasite is laterally segmented at different scales (Fig. 5E-H), indicating the pervasiveness of the deformation. The rock fabric is characterized by the presence of porphyroclasts of mafic minerals within a chloritic matrix (Fig.5I) and by S/C structures.

In calcschist, the main foliation, generally parallel to S_0 (Fig.5), is locally deformed by tight and isoclinal folds with ≈304/30 plunging hinge lines (Fig. 6A-B). These folds, characterised by the lack of an axial plane foliation, account for thermal conditions favoring plastic behavior. The stretching lineation is well defined by elongated calcite crystals, NW-SE trending (Fig. 6C). The mineral association (Fig. 6D) on main schistosity is made up of *Cal+Dol+Qtz+Bt+Ms+Chl±Ti-FeOxides±Ab±Ap±Ep* (mineral abbreviations after Kretz, 1983 and Bucher and Frey, 1994). Close to this study outcrop (Fig.4), few tens of meter southwards, muscovite on the main foliation has been dated through $^{40}Ar/^{39}Ar$ method at 19.68±0.15 Ma (Deino et al., 1992). A new deformation episode affected the previous structures, determining local open and SE-verging folds.

4. evidence of HP metamorphism

Main evidence of high-P and low-T metamorphic conditions are from the metabasite embedded in the calcschist. The nature of the parental material of the metabasite was ascertained by XRF analyses for three rock samples. Results in Table 1 indicate low contents in SiO_2 (down to 43.60 wt. %) and K_2O (down to 0.56 wt. %) and high contents in MgO (up to 9.92 wt. %) and Na_2O (up to 3.49 wt. %). Finally, a wide variation in CaO (from 6.28 to 12.36 wt. %) and elevated values of L.O.I. (up to 9.25 wt. %) can be noted. Classification of these rocks was performed by the Winchester and Floyd (1977) diagram based on immobile elements distribution, as modified by Pearce (1996; 2014). In Fig. 7, the analysed rocks are in the field of basalt, near the boundaries with the andesite/basaltic andesite and alkali basalt fields, resulting different from N-MORB and the well known ophiolitic lavas of Troodos and Semail (Pierce, 2014). The mineralogical composition of the metabasite includes *Gln+Cpx+Ep+Ab+Act+Qtz+Ilm±Ti-oxide±Spn*. It is indicative of former equilibration in the epidote blueschist subfacies (Evans, 1990) and later retrogression in the greenschist facies. Metabasite has a fine grain size and sometimes a mylonitic fabric characterized by clinopyroxene porphyroclasts set in a matrix mainly made up of glaucophane and epidote + chlorite. Clinopyroxene porphyroclasts are typically rounded and fragmented (Fig.8A-C), probably representing relics of former magmatic diopside and augite. They usually appear brownish and rare portions apparently unaffected by alteration characterized by bright interference colors. Elongated glaucophane crystals, recognizable for the pale lavender color shades, are preferentially oriented along the main foliation (Fig.8C) and wrap around clinopyroxene porphyroclasts (Fig.8D). Glaucophane is present also in the strain shadows and in the fractures of the stretched porphyroclasts (Fig.8A-B). Epidote occurs in minor amounts with respect to glaucophane and is represented by small grains, occasionally with lamellar twinning, of both clinozoisite and pistacite. It is occasionally zoned with clinozoisite cores and pistacite rims, a texture reflecting the transition to lower pressure conditions. Ilmenite and, if present, Ti-oxide, are scattered throughout the rock, showing a variable grain size. Sometimes, ilmenite can be surrounded by sphene (Fig. 8E). Rock portions characterized by the abundance of chlorite, epidote, sphene and Ti-oxide, when glaucophane and clinopyroxene relics are scarce (Fig.8E), indicate that later retrogression was non-pervasive and took place in the greenschist facies (Fig.8E). Another common textural evidence of retrogression is represented by albite blasts enclosing glaucophane and by the presence of calcite±actinolite veins crosscutting the main foliation (Fig. 8F).

In Table 2 microprobe analyses and structural formulae of selected minerals, representative of the metabasite assemblage in sample C19, are provided. We focus hereafter on those mineral phases (*i.e.*: glaucophane, clinopyroxene, epidote) used to constrain the P-T conditions of the epidote blueschist subfacies metamorphism.

Blue-amphibole nomenclature was defined according to Leake (1997) by using the software Probe-Amph (Tindle et al., 1994). It was established that all Na-amphibole analyses can be attributed to glaucophane (Fig.9A). Content in glaucophane molecula X_{Gln}, calculated as $Al^{VI}/[Fe^{3+} + Al^{VI}]$ ranges from 0.65 to 0.86. Ca-amphibole analyses are related to Fe-actinolite with average X_{Mg} of 0.78.

Clinopyroxene nomenclature was defined following Morimoto et al. (1988) and using the PX-NOM software (Sturm, 2002). Clinopyroxene porphyroclasts surrounded by glaucophane fibres can be classified in most cases as omphacite and secondly as aegirine-augite (Fig. 9B). For these types, content in jadeite molecula ranges from 0.24 to 0.33, indicating their involvement in the high-pressure metamorphic reactions. However, a smaller number of analyses, generally pertaining to isolated porphyroclasts (Fig.9C) without external glaucophane fibres, can be classified as diopside (average X_{Mg}=0.80) and, in one case, as augite (X_{Mg}=0.65). Therefore, they can be ascribed to magmatic clinopyroxene relics. Epidote is represented by both clinozoisite- and pistacite-rich terms. The content in pistacite molecula (X_{Ps}) has been calculated by Fe/[(Al-4)+Fe] on the basis of ∑O =25. It results that clinozoisite is characterized by a minimum value of X_{Ps}= 0.09 and pistacite by a maximum value of X_{Ps} = 0.82. Interestingly, in the matrix of two metabasites, microanalyses allowed to recognize the presence of anorthite with composition very close to pure calcic plagioclase end-member (Table 2). Anorthite was probably generated from a former lawsonite in response to the later heating produced at low-P conditions by the emplacement of the Porto Azzurro monzogranite pluton, as an effect of the reaction lawsonite=anorthite+H_20.

The mineral compositional data from metabasite were used for a preliminary estimation of the P-T conditions in the epidote-blueschist metamorphic subfacies. To this end, we considered the pyroxene porphyroclasts with omphacite composition (max X_{Jd} = 0.33) and glaucophane (max X_{Gln} = 0.86).

We firstly used the approach described by Sturm (2002) based on the albite =jadeite + quartz equilibrium, experimentally determined by Holland (1980). This calibration was obtained for temperatures higher than blueschist facies but, according to Sturm (2002), extrapolation to lower temperatures produces small uncertainties in P values and can provide acceptable preliminary estimates. Therefore, considering the maximum content of jadeite molecula (X_{Jd}=0.33) in omphacite, pressure values ranging from 0.95 to 1.10 GPa are obtained if the field of the epidote blueschists subfacies by Tsujimori and Ernst (2013) is considered (Fig.10). Indeed, the relatively low content of epidote in the metabasite and the suspected former presence of lawsonite, now replaced by anorthite, point to a peak P-T condition in the neighbourhood of the transition from lawsonite- to epidote-blueschist subfacies. According to Zhang et al. (2009), blueschists of NW China crossed this transition during subduction at temperatures close to 350 °C. In Fig.10 the isopleth related to the observed maximum content in jadeite molecula meets the transition line between the two subfacies at a T of *c*. 330 °C, corresponding to a pressure of *c*. 0.95 GPa. Lower P estimates (Fig.10) are obtained on the basis of the Na-amphibole composition. By following the calibration of Maruyama et al. (1986) and by plotting the isopleth related to the maximum content in glaucophane molecula in the field of epidote blueschist subfacies, a value of pressure slightly above 0.7 GPa is estimated. This result may indicate that, after the peak pressure condition, glaucophane re-equilibrated in a later stage during the exhumation.

A confirmation of the high-pressure metamorphic event was obtained from SEM-EDS analyses revealing the presence of white mica (Fig. 11A) with an elevated content in celadonite molecula (X_{Cel}=0.5 and Si=3.5 a.p.f.u.) in metabasite sample RMT3 (Table 3). However, although it accounts for high-P conditions, the lack of a limiting mineral assemblage in equilibrium with phengite (*i.e.*: K-feldspar, quartz, Mg/Fe silicates) precludes quantifying pressure by a geobarometric approach.

Another indication in favor of the high-pressure metamorphism comes from a phengite-bearing quartzite (sample RIO6B) in the Torre Giove locality (Fig. 2, 11B and Table 3). The main schistosity is defined by Qtz+Ms+ Kln±Cal ± Fe-Ti oxide. In some cases, detrital grains of white mica are surrounded by aggregates of newly-formed flakes of phengite (Fig. 11B) with Si content of about 3.5 a.p.f.u. (Table 3).

5. Discussion and Conclusions

The metasedimentary succession where we have found metabasite, has been differently interpreted through time. According to Trevisan (1950), Barberi et al. (1969), Perrin (1975) and Keller and Pialli (1990), it is considered as part of the sedimentary succession belonging to the Tuscan Domain. Differently, Duranti et al. (1992) and Pertusati et al. (1993) interpreted the ophiolite slice (*i.e.* the oceanic unit 1 in Fig. 3) and the underlying metasedimentary succession, where the study metabasite is embedded, as belonging to the same overturned Jurassic-Cretaceous oceanic succession of the inner Ligurian Domain (Pertusati et al., 1993). This unit was later affected by contact metamorphism during the emplacement of the Porto Azzurro monzogranite (Duranti et al., 1992). Pandeli et al. (2001) followed this interpretation and suggested that this succession can be related to the Piedmont Ocean sedimentary evolution.

Our data indicate that the composition of the metabasite rocks (Fig.7) is not compatible with an oceanic setting, *i.e.* the Ligurian-Piedmont Ocean. Thus, we sustain that the hosting metasediments cannot be related to the sedimentary succession of the ophiolite slice (oceanic unit 1 in Fig. 3). The latter instead is tectonically located above the calcschist (Fig.2). As a consequence, and as already proposed by the previously cited Authors, the metasedimentary succession under discussion should be linked to the Tuscan domain (Fig.3).

Mineral association and P-T conditions indicate an equilibration of the metabasite in the epidote blueschist subfacies with a pressure peak of 0.9-1.0 GPa. Metamorphic studies (Fig.1) carried out in the inner Northern Apennines indicate an eastward decrease of pressure (Rossetti et al. 2002 with references therein), from 1.3-1.6 GPa (Gorgona and Giglio Islands, Fig.1) to 0.8-1.0 GPa (southern Tuscany), as obtained on metasediments with Fe-Mg silicates (Giorgetti et al., 1998; Rossetti et al, 1999; Rossetti et al., 2001; Agard et al., 2000).

A comparison between P-values obtained for metasediment and metabasite parageneses from other localities of inner Northern Apennines (Fig.1), indicates that the metamorphic peak in metabasites is encompassed between 0.6 and 0.8 GPa (T= 275-350°C). Instead, P-values obtained from metasediments range from 0.8 to 1.5 GPa (T=350-420°C) in six out of seven localities. Thus it can be inferred that metabasites usually provide peak estimates lower than metasediments.

Although in the Elba Island pressure estimate is slightly higher (P=0.9-1.0 Gpa; T=330-350°C) than those obtained for the other metabasites, we interpret all the barometric values in the same tectono-metamorphic framework of the inner Northern Apennines. On this basis, the result provided by the Elba Island metabasite has two significant implications: (i) the tectonic stacking of the Elba Island units did not occur in a low-P context, as supposed by Pertusati et al. (1993) and, more recently, by Musumeci and Vaselli (2012); (ii) the Elba Island is now reconciled in the tectonic and metamorphic evolution of the Northern Apennines. Furthermore, it results that its stratigraphic and metamorphic evolution is significantly similar to the one described for the Gorgona Island, suggesting that the interpretation of the Gorgona calcschist as a part of the Piedmont Ocean (Capponi et al., 1990; Pandeli et al., 2001; Rossetti et al., 2001) should be revised.

Finally, considering reasonable that the high content of Si in phengite from the Monte Giove area is a further evidence of high-P conditions, it derives that continental units 2 and 3 (Fig. 3) have been affected by high P-metamorphism too. Consequently, it can be inferred that also the oceanic unit 1, interposed between the continental unit 2 and 3 (Fig.3 and 4), underwent metamorphism in high-P conditions. The absence of a corresponding paragenesis, is probably an effect of the thermal perturbation produced by the emplacement of the Porto Azzurro monzogranite (Pertusati et al., 1993; Bortolotti et al., 1994).

As it regards the timing of metamorphism, we have in the area two different radiometric ages: Brunet et al. (2000) dated muscovite on the main schistosity of calcschist cropping out in the Gorgona Island (Fig.1), obtaining 25.5±0.3 Ma by $^{40}Ar/^{39}Ar$ geochronology; by the same method, Deino et al. (1992) dated the muscovite, grown on the main schistosity of the calcschist of the Elba Island (Fig.4), providing a radiometric age of 19.68±0.15 Ma. Assuming that the study metabasite and hosting calcschist record the same deformational event and considering that both glaucophane in metabasite, and white mica in calcschist, are syn-kynematic, we suggest that the radiometric ages are indicative for the high-P metamorphic event. We can therefore assess that the high-P conditions occurred during the late Oligocene-early Burdigalian time interval.

ACKNOWLEDGMENTS

The research leading to these results has received funding from the European

Community's Seventh Framework Programme under grant agreement No. 608553 (Project IMAGE).

REFERENCES

Agard, P., Goffé, B., Touret, J.L.R., Vidal, O., 2000. Retrograde fluid evolution in blueschist-facies metapelites (Schistes lustrés unit, Western Alps). Contrib. Mineral. Petr. 140, 296–315.

Baldi, P., Bertini, G., Cameli, G.M., Decandia, F.A., Dini, I., Lazzarotto, A., Liotta, D., 1994. Tettonica distensiva post-collisionale nell'area geotermica di Larderello (Toscana meridionale). Studi Geologici Camerti Spec 1, 183–193.

Balestrieri, M.L., Pandeli, E., Bigazzi, G., Carosi, R., Montomoli, C., 2011. Age and temperature constraints on metamorphism and exhumation of the syn-orogenic metamorphic complexes of Northern Apennines, Italy. Tectonophysics, 509, 254-271.

Barberi, F., Dallan, L., Franzini, M., Giglia, G., Innocenti, F., Marinelli, G., Raggi, R., Ricci, C.A., Squarci, P., Taffi, L., Trevisan, L., 1969. Note illustrative della Carta Geologica d' Italia alla scala 1:100.000, Foglio 126 (Isola d'Elba). Serv. Geol. d'It., 32 pp.

Barberi, F., Innocenti, F., 1965. Le rocce cornubianitico-calcaree dell'anello termometamorfico del Monte Capanne (Isola d'Elba). Atti Soc. Tosc. Sci. Nat., Mem., Ser. A 72, 306-398.

Barchi, M.R., 2010. The Neogene-Quaternary evolution of the Northern Apennines: crustal structure, style of deformation and seismicity. In: Beltrando, M., Peccerillo, A., Mattei, M., Conticelli, S., Doglioni, C. (Eds.): The Neogene–Quaternary evolution of the Northern Apennines: crustal structure, style of deformation and seismicity. Journ. Virt. Explorer 36, doi:10.3809/jvirtex.2009.00220.

Bertini, G., Cameli, G.M., Costantini, A., Decandia, F.A., Di Filippo, M., Dini, I., Elter, F.M., Lazzarotto, A., Liotta, D., Pandeli, E., Sandrelli, F., Toro, B., 1991. Struttura geologica fra i monti di Campiglia e Rapolano Terme (Toscana meridionale): stato attuale delle conoscenze e problematiche. Studi Geol. Camerti 1, 155–178.

Bonini, M., Sani, F., Stucchi, E.M., Moratti, G., Benvenuti, M., Menanno, G., Tanini, C., 2014. Late Miocene shortening of the Northern Apennines back-arc. J. Geodynamics 74, 1-31.

Bortolotti, V., Cellai, D., Martin, S., Principi, G., Tartarotti, P., Vaggelli, G., 1994. Ultramafic rocks from the eastern Elba island ophiolites (Tyrrhenian Sea, Italy). Mem. Soc. Geol. It. 48, 195-202.

Bortolotti, V., Fazzuoli, M., Pandeli, F., Principi, G., Babbini, A., Corti, S., 2001. Geology of Central and Eastern Elba Island, Italy. Ofioliti 26, 97-150.

Bossio, A., Costantini, A., Lazzarotto, A., Liotta, D., Mazzanti, R., Mazzei, R., Salvatorini, G.F., Sandrelli, F., 1993. Rassegna delle conoscenze sulla stratigrafia del Neoautoctono toscano. Mem. Soc. Geol. It. 49, 17–98.

Brogi, A., Giorgetti,G., 2012. Tectono-metamorphic evolution of the siliciclastic units in the Middle Tuscan Range (inner Northern Apennines): Mg–carpholite bearing quartz veins related to syn-metamorphic syn-orogenic foliation. Tectonophysics, 526–529 (2012) 167–184.

Brogi, A., Liotta, D., 2008. Highly extended terrains, lateral segmentation of the substratum, and basin development: the Middle–Late Miocene Radicondoli Basin (inner northern Apennines, Italy). Tectonics 27. doi:10.1029/2007TC002188 TC 5002.

Brunet, C., Monie, P., Jolivet, L., Cadet, J.P., 2000. Migration of compression and extension in the Tyrrhenian sea, insights from $^{40}Ar/^{39}Ar$ ages on micas along a transect from Corsica to Tuscany. Tectonophysics 321, 127–155.

Bucher, K., Frey, M., 1994. Petrogenesis of metamorphic rocks. Springer-Verlag, Berlin, 318 pages.

Butler, R.W.H., 1987. Thrust sequences. Journ. Geol. Soc. London 144, 619-634.

Caggianelli, A., Ranalli, G., La Vecchia, A., Liotta, D., Dini, A., 2014. Post-emplacement thermo-rheological history of a granite intrusion and surrounding rocks: the Monte Capanne pluton, Elba Island, Italy. From: Llana-Fúnez, S., Marcos, A. & Bastida, F. (eds) Deformation Structures and Processes within the Continental Crust. Geological Society, London, Special Publications, 394, 129-143.

Capponi, G., Giammarino, S., Mazzanti, R., 1990. Geologia e morfologia dell'Isola di Gorgona. Quad. Mus. Stor.Nat. Livorno 11, 115-137

Carmignani, L., Decandia, F.A., Disperati, L., Fantozzi, P.L., Lazzarotto, A., Liotta, D., Meccheri, M., 1994. Tertiary extensional tectonics in Tuscany (Northern Apenines, Italy). Tectonophysics 238, 295–315.

Carmignani, L., Decandia, F.A., Disperati, L., Fantozzi, P.L., Lazzarotto, A., Liotta, D., Oggiano, G., 1995. Relationships between the Sardinia-Corsica-Provencal Domainand the Northern Apennines. Terranova 7, 128–137.

Carmignani, L., Kligfield, R., 1990. Crustal extension in the Northern Apennines: the transition from compression to extension in the Alpi Apuane core complex. Tectonics, 9, 1275-1303.

Chemenda, A.I., Mattauer, M., Malavieille, J., Bokun, A., 1995. A mechanism for syncollisional rock exhumation and associated normal faulting: results from physical modelling. Earth Plan. Sc. Lett. 132, 225–232.

Crawford, W.A., Fyfe, W.S., 1965. Lawsonite equilibria. Am. J. Sci. 263, 262-270.

Deino, A., Keller, J.V.A., Minelli, G., Pialli, G., 1992. Datazioni ^{39}Ar/^{40}Ar del metamorfismo dell'Unità di Ortano-Rio Marina (Isola d'Elba): risultati preliminari. Studi Geol. Camerti 1, 187–192.

Dini, A., Innocenti, F., Rocchi, S., Tonarini, S., Westerman, D.S., 2002. The magmatic evolution of the Late Miocene laccolith–pluton–dyke granitic complex of Elba Island, Italy. Geol. Mag. 139, 257–279.

Duranti, S., Palmieri, R., Pertusati, P.C., Ricci, C.A., 1992. Geological evolution and metamorphic petrology of the basal sequences of eastern Elba (Complex II). Acta Vulcanologica 2, 213-229.

Elter FM., Pandeli E. 2002. The HP-LP meta-ophiolitic unit and Verrucano of the Cala Grande Area in the Argentario Promontory (southern Tuscany, Italy): structural metamorphic evolution and regional considerations. Ofioliti, 27(2), 91-102.

Evans, B.W., 1990. Phase relations of epidote-blueschists. Lithos 25, 3–23.

Garfagnoli, F., Menna, F., Pandeli, E., Principi, G., 2005. The Porto Azzurro Unit (Mt. Calamita promontory, south-eastern Elba Island, Tuscany): stratigraphic, tectonic and metamorphic evolution. Boll. Soc. Geol. It. 3, 119-138.

Giorgetti, G., Goffé, B., Memmi, I., Nieto, F., 1998. Metamorphic evolution of Verrucano metasediments in northern Apennines: new petrological constraints. Eur. Journ. Miner. 10, 1295–1308.

Holland, T.J. B., 1980. The reaction albite=jadeite + quartz determined experimentally in the range 600°-1200°C. Am. Miner. 65, 129-134.

Jolivet, L., Dubois, R., Fournier, R., Goffe', B., Michard, A., Jourdan, C., 1990. Ductile extension in alpine Corsica. Geology 18, 1007–1010.

Jolivet, L., Faccenna C., Goffé, G., Burov, E., Agard, P., 2003. Subduction tectonics and exhumation of high-pressure metamorphic rocks in the mediterranean orogens. Am. J. Sci. 303, 353-409.

Jolivet, L., Goffé, B., Truffert-Luxey, C., Patriat, M., Bonneau, M. 1996. Miocene detachment in Crete and exhumation P-T-t paths of high-pressure metamorphic rocks. Tectonics 15, 1129-1153.

Jolivet, L., Faccenna, C., Goffé, B., Mattei, M., Rossetti, F., Brunet, C., Storti, F., Funiciello, R., Cadet, J.P., D'Agostino, N., Parra, T., 1998. Midcrustal shear zones in postorogenic extension: example from the northern Tyrrhenian Sea. J. Geophys. Res. 103 (B6), 12123–12160.

Keller, J.V.A., Pialli, G., 1990. Tectonics of the island of Elba: a reappraisal. Boll. Soc. Geol. It. 109, 413–425.

Keller, JVA, Coward, MP., 1996. The structure and evolution of the Northern Tyrrhenian Sea. Geol. Magazine 133, 1-16.

Kligfield, R., Hunziker, J., Dallmayer, R.D., Schamel, S., 1986. Dating of deformation phases using K-Ar and $^{40}Ar/^{39}Ar$ techniques: results from the Northern Apennines. J. Struct. Geol. 8, 781-798.

Kretz, R., 1983. Symbols for rock-forming minerals. Am. Mineral. 68, 277-279.

Leake, BE., Woolley, AR., Arps, C.E.S., Birch, W.D., Gilbert, M.C., Grice, J.D, Hawthorne, F.C., Kato, A., Kisch, H.J, Krivovichev, V.G., Linthout, K., Laird, J., Mandarino, J.A., Maresch, W.V., Nickel, E.H., Rock, N.M.S., Schumacher, JC; Smith, DC; Stephenson, N.C.N., Ungaretti, L., Whittaker, E.J.W., Guo, Y.Z., 1997. Nomenclature of amphiboles: Report of the subcommittee on amphiboles of the International Mineralogical Association, commission on new minerals and mineral names. Am. Mineral. 82, 1019-1037.

Maresch, W.V., 1977. Experimental studies on glaucophane: an analysis of present knowledge. Tectonophysics 43, 109-125.

Maruyama, S., Cho, M., Liou, J.G., 1986. Experimental investigations of blueschist-greenschist transition equilibria: Pressure dependence of Al_2O_3 contents in sodic amphiboles- a new geobarometer. Geol. Soc. Am. Memor 164, 1-16.

Maineri, C., Benvenuti, M., Costagliola, P. Dini, A., Lattanzi, P., Ruggieri, G., Villa, I.M., 2003. Sericitic alteration at the La Crocetta deposit (Elba Island, Italy): interplay between magmatism, tectonics and hydrothermal activity. Mineralium Deposita 38, 67-86.

Molli, G., 2008. Northern Apennine–Corsica orogenic system: an updated overview. Geol. Soc. London, Spec. Publ. 298, 413–442.

Morimoto, N., Fabries, J., Ferguson, A.K., Ginzburg, R.M., Seifert, F., Zussman, J., Aoki, K., Gottardi, G., 1988. Nomenclature of Pyroxenes. Am. Mineral. 73, 1123-1133.

Musumeci, G., Mazzarini, F., Tiepolo, M., Di Vincenzo, G., 2011. U-Pb and ^{40}Ar-^{39}Ar geochronology of Palaeozoic units in the Northern Apennines: determining protolith age and alpine evolution using the Calamita Schist and Ortano Porphyroids. Geol. J. 46, 288–310.

Musumeci, G., Vaselli, L., 2012. Neogene deformation and granite emplacement in the metamorphic units of northern Apennines (Italy): Insights from mylonitic marbles in the Porto Azzurro pluton contact aureole (Elba Island). Geosphere 8, 470–490.

Pandeli, E., Puxeddu, M., Ruggieri, G., 2001. The metasiliciclastic-carbonate sequence of the Acquadolce Unit (eastern Elba Island): new petrographic data and palaeogeographic interpretation. Ofioliti 26, 207-218.

Pearce, J.A., 1996. A user's guide to basalt discrimination diagrams. In: Wyman, D. A. (Eds.), Trace element geochemistry of volcanic rocks; applications for massive sulphide exploration. Geol. Ass. Canada, Short Course Notes 12, 79-113.

Pearce, J.A., 2014. Immobile elements finger printing of ophiolite. Elements 10, 101-108.

Peccerillo, A., 2003. Plio-Quaternary magmatism in Italy. Episodes 26, 222–226.

Perrin, M., 1975. L'ile d'Elbe et la limite Alpes-Apennin: données sur la structure géologique et l'évolution tectogenétique de l'Elbe Alpine et de l'Elbe Apennine. Boll. Soc. Geol. It. 94, 1929-1955.

Pertusati, P., Raggi, G., Ricci, C.A., Duranti, S., Palmeri, R., 1993. Evoluzione post-collisionale dell'Elba centro-orientale. Mem. Soc. Geol. It. 49, 297–312.

Rossetti, F., Faccenna, C., Jolivet, L., Funiciello, R., Tecce, F., Brunet, C., 1999. Syn- versus post-orogenic extension: the case study of Giglio Island (Northern Tyrrenian Sea, Italy). Tectonophysics 304, 73–92.

Rossetti, F., Faccenna, C., Jolivet, L., Funiciello, R., Goffè, B., Tecce, F., Brunet, C., Monié, P., Vidal, O., 2001. Structural signature and exhumation P–T–t path of the Gorgona blueschist sequence (Tuscan Archipelago, Italy). Ofioliti 26, 175–186.

Rossetti, F., Faccenna, C., Jolivet, L., Goffé, B., Funiciello, R., 2002. Structural signature and exhumation P–T–t paths of the blueschist units exposed in the interior of the Northern Apennine chain, tectonic implications. Boll. Soc. Geol. It. 1, 829–842.

Rossetti, F., Glodny, J., Theye, T., Maggi, M., 2015. Pressure-Temperature-deformation-time of the ductile Alpine shearing in Corsica: from orogenic construction to collapse, LITHOS, doi: 10.1016/j.lithos.2015.01.011

Rossetti, F., Tecce, F., Billi, A., Brilli, M., 2007. Patterns of fluid flow in the contact aureole of the Late Miocene Monte Capanne pluton (Elba Island, Italy): the role of structures and rheology. Contrib. Mineral. Petrol. 153, 743-760.

Sturm, R., 2002. PX-NOM—an interactive spreadsheet program for the computation of pyroxene analyses derived from the electron microprobe. Computers & Geosciences 28, 473–483.

Tanelli, G., 1983. Mineralizzazioni metallifere e minerogenesi della Toscana. Mem. Soc. Geol. It. 25, 91–109.

Tanelli, G., Benvenuti, M., Costagliola, P., Dini, A., Lattanzi, P., Manieri, C., Mascaro, I., Ruggieri, G., 2001. The iron mineral deposits of Elba Island: state of the art. Ofioliti 26, 239-248.

Theye, T., Reinhardt, J., Goffè, B., Jolivet, L., Brunet, C., 1997. Fe- and Mg-carpholite from the Monte Argentario (Italy): first evidence for high-pressure metamorphism of the metasedimentary Verrucano sequence, and significance for P–T path reconstruction. Eur. Journ. Miner. 9, 859–873.

Tindle, A.G., Webb, P.C., 1994. Probe-AMPH—A spreadsheet program to classify microprobe-derived amphibole analyses. Computers & Geosciences 20, 1201-1228.

Tsujimori, T., Ernst, W.G., 2013. Lawsonite blueschists and lawsonite eclogites as proxies for palaeo-subduction zone processes: a review. J. Metam. Geol. doi:10.1111/jmg.12057.

Trevisan, L., 1950. L'Elba orientale e la sua tettonica di scivolamento per gravità. Mem. Ist. Geol. Univ. Padova 16, 1–30.

Wei, C.J., Clarke, G.L., 2011. Calculated phase equilibria for MORB compositions: a reappraisal of the metamorphic evolution of lawsonite eclogite. J. met. Geol. 29, 939–952.

Westerman, D.S., Dini, A., Innocenti, F., Rocchi, S., 2004. Rise and fall of a nested Christmas-tree laccolith complex, Elba Island, Italy.In: Breitkreuz, C., Petford, N. (Eds): Physical Geology of High-Level Magmatic Systems. Geol. Soc. London, Spec. Publ. 234, 195-213.

Winchester, J.A., Floyd, P.A., 1977. Geochemical discrimination if different magma series and their differentiation products using immobile elements. Chem. Geol. 20, 325-343.

Zhang, Z.C., Mao, J.W., Saunders, A.D., Ai, Y., Li, Y., Zhao, L., 2009. Petrogenetic modeling of three mafic-ultramafic layered intrusions in the Emeishan large igneous province, SW China, based on isotopic and bulk chemical constraints. Lithos 113, 369-392.

CAPTIONS

Figure 1 - Structural sketch map of Tuscany (inner Northern Apennines) with location of the HP-LT mineralogical assemblages in metabasite (black circle) and other rock types (metasediments). The P-T values from Rio Marina (no.11) are presented in this paper; other data Kligfield et al. (1986); Theye et al. (1997); Giorgetti et al. (1998); Rossetti et al. (1999); Brunet et al. (2000); Rossetti et al. (2001); Elter and Pandeli, (2001); Brogi and Giorgetti (2012).

Figure 2 - Geological sketch map of the Elba Island. The relationships between the tectonic units are highlighted as described in the text. The location of the phengite -and glaucophane-bearing rocks is also indicated.

Figure 3 – Tectono-stratigraphic columns showing the seven tectonic units belonging both to continental and oceanic environments and forming the tectonic pile of the Elba Island. From right to left, and from the bottom in each column: oceanic unit 3: bΣ = Breccia of ophiolitic rocks; LC = limestone and shale (Palombini Shales Fm); C = shale (Varicoluored shales Fm); S = sandstone and shale (Ghiaieto Sandstones Fm); Sc = sandstone and marlstone (Marina di Campo Fm); Ts = shale with limestone and marlstone (Colle Reciso Fm). Oceanic unit 2: Σ = ophiolite; J = radiolarite (Mt. Alpe Cherts Fm); Cl = calcilutite and cherty limestone (Nisportino Fm); L = cherty limestone (Calpionella Limestones Fm); LC

= limestone and shale (Palombini Shales Fm). Continental unit 4: Ev = Evaporite (Calcare Cavernoso Fm); M = massive and cherty limestone and dolostone (Pania di Corfino Fm, Mt. Cetona Fm, Calcare Massiccio Fm, Grotta Giusti Limestones, Rosso Ammonitico Fm, Limano cherty Limestones Fms); Mp= marls (Posidonia Marlstones Fm); Ml = varicolored shales (Cavo Fm). Continental unit 3: Bphy = black phyllite (Rio Marina Fm); Q = quartzite and phyllite (Verruca Fm, Mt. Serra quartzite Fm); M = marble (Valle Giove Limestones Fm; Capo Pero Limestone Fm; Capo Castello Calcschists Fm); Mc = cherty marble; Cs = calcschist and phyllite (Varicoloured Sericitic Schist Fm); Ms = metasandstone and phyllite (Pseudomacigno Fm). Continental unit 2: P = porphyroids, quartzite and phyllite (Ortano Unit); Q = quartzite; M = massive and cherty limestone and dolostone (Valdana marble Fm); Mp = marls (Posidonia Marlstones Fm); J = radiolarite; Phy = calcschist with interbedded metabasite (Mb) and phyllite (Acquadolce Unit). Oceanic unit 1: Σ = ophiolite. Continental unit 1: Mc = micaschist (Mt. Calamita Fm); Q = quartzite and phyllite (Quarziti di Barabarca Fm); M = dolostone (Crystalline dolostone and dolomitic limestone Fm). Formational names after Bortolotti et al. (2001) and Garfagnoli et al. (2005). The stars indicate the location of the analysed samples.

Figure 4 - Geological map and cross sections of the Rio Marina area.

Figure 5 - A) panoramic view of the sampling area; B) lenses of metabasite embedded in calcshist; C) metabasites lenses located mainly along the main schistosity, gently NW-dipping; D) detail of metabasite lens; E-H) metabasite laterally segmented at different scales indicating the pervasiveness of the deformation; I) rock fabric characterized by the presence of porphyroclasts of mafic minerals within a chloritic matrix.

Figure 6 - A-B) tight and isoclinal folds with ≈304/30 plunging hinge lines deforming the meian foliation in calcschists; C) stretching lineation well defined by elongated calcite crystals, NW-SE trending; D) SEM-BSE (scanning electron microscopy-back scattered electron) image showing the textural characteristics and paragenesis of micaschists. Mineral abbreviations after after Kretz (1983) and Bucher and Frey (1994). D) SEM-BSE (scanning electron microscopy-back scattered electron) image showing the textural characteristics and paragenesis of micaschists. Mineral abbreviations after after Kretz (1983) and Bucher and Frey (1994).

Figure 7 - Immobile elements TAS proxy diagram (Pearce, 2014). Grey area indicates the field of ophiolitic lavas from Troodos (Cyprus) and Semail (Oman) as reported by Pearce (2014). The metabasite under study (white circles) in comparison to Troodos and Semail lavas show a more pronounced alkaline affinity.

Figure 8 - Micrographs of a metabasite sample (plane polarised light in A-E and crossed polars in F). A) Rounded porphyroclast of clinopyroxene with strain shadow filled by glaucophane; B) Stretched and fractured porphyroclast of clinopyroxene. Fracture is filled by glaucophane fibres grown parallel to the stretching direction; C) Elongated well-developed glaucophane crystals, mostly oriented along the main foliation between clinopyroxene porphyroclasts; D) Glaucophane fibres wrapping around porfiroclasts of clinopyroxene; E) Rock portion affected by retrogression in greenschist facies as shown by the widespread chlorite and by the corona of sphene around ilmenite; F) Late calcite

vein cross-cutting at high angle the main foliation. Mineral symbols from Kretz (1983).

Figure 9 - A) Classification diagram of Na-Amphiboles in metabasite (after Leake et al., 1997). B) Classification diagram for Ca-Na pyroxenes in the metabasite according to Morimoto et al. (1988); Q = wollastonite+enstatite+Ferrosilite. C) Classification diagram for Ca-Fe-Mg pyroxenes in the metabasite by Morimoto et al. (1988).

Figure 10 - P-T diagram showing approximate metamorphic conditions (circles) for the Elba Island blueschists constrained by mineral assemblage and composition of omphacite (yellow) and glaucophane (lilac). X_{Jd} isopleth calculated with the aid of the Sturm (2002) software on the basis of Ab = Jd + Qtz equilibrium calibrated by Holland (1980). X_{Gln} isopleth from calibration by Maruyamaet al. (1986). Subfacies boundaries by Tsujimori and Ernst (2013) and some relevant equilibria have been shown. Metamorphic facies and sub-facies abbreviations: L-Bs = lawsonite blueschist; E-Bs = epidote blueschist; Gs = greenschist; E-Am = epidote - amphibolite; Am = amphibolite; Amph-Ec = amphibole eclogite. Mineral stability boundary and equilibria: Gln-in = stability boundary of glaucophane by Maresch (1977); Omph-in = stability boundary of omphacite-in a jadeite-enriched MORB (MORB+ in Tsujimori and Ernst, 2013); Ab = Jd + Qtz by Tsujimori and Ernst (2013); Lws = An + H_2O by Crawford and Fyfe (1965). Mineral abbreviations according to Kretz (1983).

Figure 11 - SEM-BSE (scanning electron microscopy-back scattered electron) images: A) RMT3 metabasite sample with glaucophane (Gln), clinopyroxene (Cpx) and

phengite (Phe). B) Phengite (Phn) from Torre Giove quartzite; phengite is more celadonite -rich in the rim (lighter color).

Table 1 - XRF analyses of three metabasites samples.

Table 2 - Representative analyses of Metabasite (sample C19). Beam width was approximately of 1 μm. Table 2. Mineral abbreviations according to Kretz (1983) and Bucher and Frey (1994): Gln=glaucophane; Act=actionolite; Omph=omphacite; Agt=aegirine-augite; Di=diopside; Aug=augite; Clz=clinozoisite; Ps=pistacite. Analyses were performed on the JEOL 8200 microprobe, at the University of Milan, operating in WDS/EDS with an accelerating voltage of 15 kV and 5 nA current. Beam width was approximately of 1 μm.

Table 3 - Selected SEM/EDS analyses of phengites in metabasite (sample RMT3) and quartzite (RIO6B). Analyses were performed on the Philips XL30 SEM at the University of Siena, operating in EDS/EDAX with an accelerating voltage of 20 kV.

finding of HP-LT metamorphism in Elba Island

implications for the geodynamic evolution of N.Apennines

revision of the tectonic units involved in the N.Appennine stacking

Table1

	C19	RMT2	RMT3
wt.%			
SiO_2	44.84	43.60	44.15
TiO_2	1.15	0.84	1.03
Al_2O_3	17.04	13.72	15.23
FeO_t	10.52	7.96	9.45
MnO	0.16	0.09	0.12
MgO	9.92	7.29	9.55
CaO	6.28	12.36	9.80
Na_2O	2.10	3.49	3.11
K_2O	0.58	1.04	0.59
P_2O_5	0.14	0.13	0.14
L.O.I.	6.86	9.25	6.68
Tot	99.58	99.75	99.85
ppm			
Ni	139	91	133
Cr	287	199	265
V	193	111	157
Rb	40	46	26
Sr	234	483	445
Ba	21	104	46
Y	24	17	22
Zr	106	91	105
Nb	8	7	7
La	23	7	10
Ce	70	27	38

Table2

	Amphiboles		Clinopyroxenes				Feldspars		Epidotes		Chlorite
	Gln	Act	Omph	Agt	Di	Aug	Ab	An	Clz	Ps	
wt.%											
SiO_2	58.08	57.28	55.20	54.00	51.63	52.13	68.36	42.51	39.27	37.87	30.03
TiO_2	0.22	0.03	0.10	0.01	1.00	0.03	0.01	0.01	0.12	0.06	0.02
Al_2O_3	9.63	1.06	7.20	3.26	2.15	4.44	19.50	36.79	32.55	22.28	20.74
Cr_2O_3		0.04	0.28	0.19	0.02				0.02	0.09	0.03
FeO_t	9.76	6.89	9.36	9.86	6.71	13.69	0.07	0.17	1.4	12.55	14.26
MnO	0.17	0.30	0.13	0.23	0.19	0.22			0.03	0.11	0.38
MgO	10.56	18.47	7.44	9.90	15.04	14.23	0.01	0.01	0.06	0.03	20.97
CaO	1.09	11.20	11.65	15.19	21.64	13.22	0.03	19.80	23.55	22.18	0.06
Na_2O	6.16	0.86	7.34	5.33	0.36	0.35	11.68	0.05	0.01	0.03	0.01
K_2O	0.02	0.03	0.04	0.04	0.03	0.11		0.03	0.01	0.02	0.08
Tot	95.68	96.14	98.74	98.01	98.76	98.42	99.66	99.37	97.02	95.22	86.58
ΣO	23	23	6	6	6	6.066	8	8	25	25	28
Si	8.063	8.087	2.011	2.004	1.929	1.982	2.994	1.982	6.027	6.320	5.986
Al^{IV}					0.071	0.018	1.008	2.024			2.014
Al^{VI}	1.576	0.176	0.309	0.143	0.024	0.181			5.895	4.387	2.864
Ti	0.022	0.004	0.003		0.028	0.001			0.014	0.008	0.003
Cr		0.004	0.008	0.006	0.001				0.002	0.012	0.005
Fe	1.133	0.813	0.289	0.306	0.210	0.435	0.003	0.007	0.180	1.751	2.377
Mn	0.020	0.036	0.004	0.007	0.006	0.007			0.004	0.016	0.064
Mg	2.190	3.885	0.404	0.558	0.838	0.806	0.001	0.001	0.014	0.007	6.231
Ca	0.163	1.693	0.455	0.604	0.866	0.538	0.001	0.989	3.872	3.966	0.013
Na	1.658	0.234	0.519	0.391	0.026	0.026	0.992	0.005	0.003	0.010	0.004
K	0.003	0.005	0.002	0.002	0.001	0.005		0.002	0.002	0.004	0.020
Fe^{3+}	0.266	0.024	0.175	0.227	0.017						
Fe^{2+}	0.867	0.789	0.110	0.079	0.193	0.435					
ΣCat	14.827	14.938	4.000	4.000	4.000	4.000	4.998	5.009	16.013	16.480	19.581
X_{Gln}	0.86										
X_{Jd}			0.33	0.15							
X_{Wo}					0.45	0.30					
X_{En}					0.47	0.45					
X_{Fs}					0.11	0.25					
X_{Q}			0.48	0.62							
X_{Ae}			0.19	0.24							
X_{Ps}									0.09	0.82	
X_{An}							0.00	1.00			
X_{Ab}							1.00	0.00			
X_{Mg}	0.72	0.83	0.70	0.88	0.81	0.65					

Table3

	Metabasite RMT3	Quartzite RIO6A
wt.%		
SiO_2	52.69	51.65
TiO_2	0.15	0.19
Al_2O_3	24.61	23.77
FeO_t	3.34	5.93
MnO	0.12	0.11
MgO	4.97	2.98
CaO	0.18	0.11
Na_2O	0.12	0.08
K_2O	9.66	10.96
Tot	95.85	95.77
∑O	11	11
Si	3.49	3.50
Al^{IV}	0.50	0.50
Al^{VI}	1.42	1.40
Ti	0.01	0.01
Fe	0.19	0.34
Mn	0.00	0.00
Mg	0.49	0.30
Ca	0.01	0.01
Na	0.01	0.01
K	0.81	0.94
∑Cat	6.95	7.02
X_{Cel}	0.50	0.50

Figure1

Click here to download high resolution image

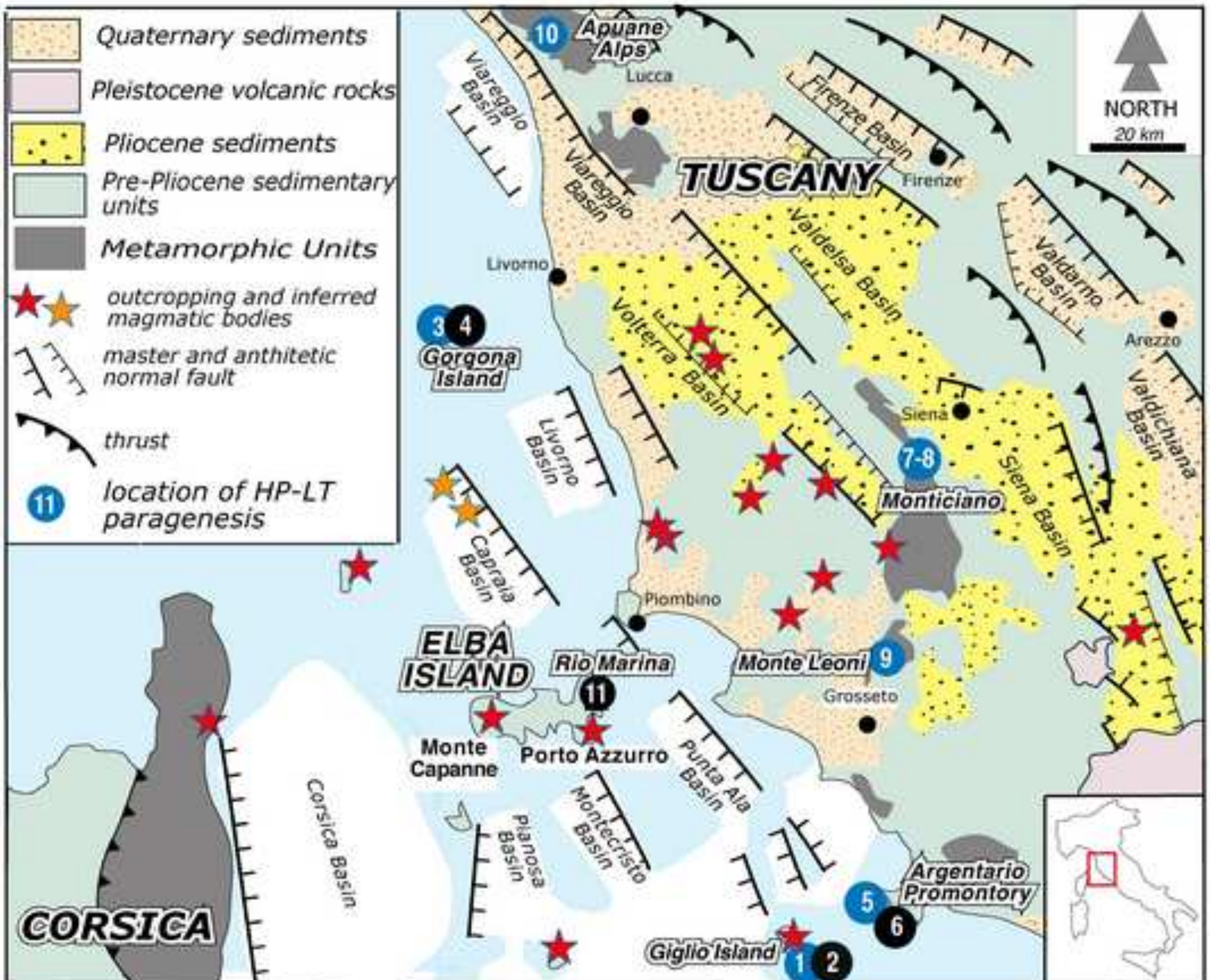

	P (GPa)	T (°C)	
1	1.0-1.4	< 350	metasediments
2	0.7-0.8	300-350	metabasite
3	1.4-1.5	< 350	metasediments
4	0.6-0.8	275-300	metabasite
5	1.0-1.1	360-380	metasediments
6	0.7-0.8	340-350	metabasite
7	1.1-1.4	370-420	metasediments
8	0.8-1.0	380-420	metasediments
9	0.8-1.0	350-380	metasediments
10	0.6-0.8	about 450	metasediments
11	0.9-1.0	300-350	metabasite

FIGURE 1

Figure2

Click here to download high resolution image

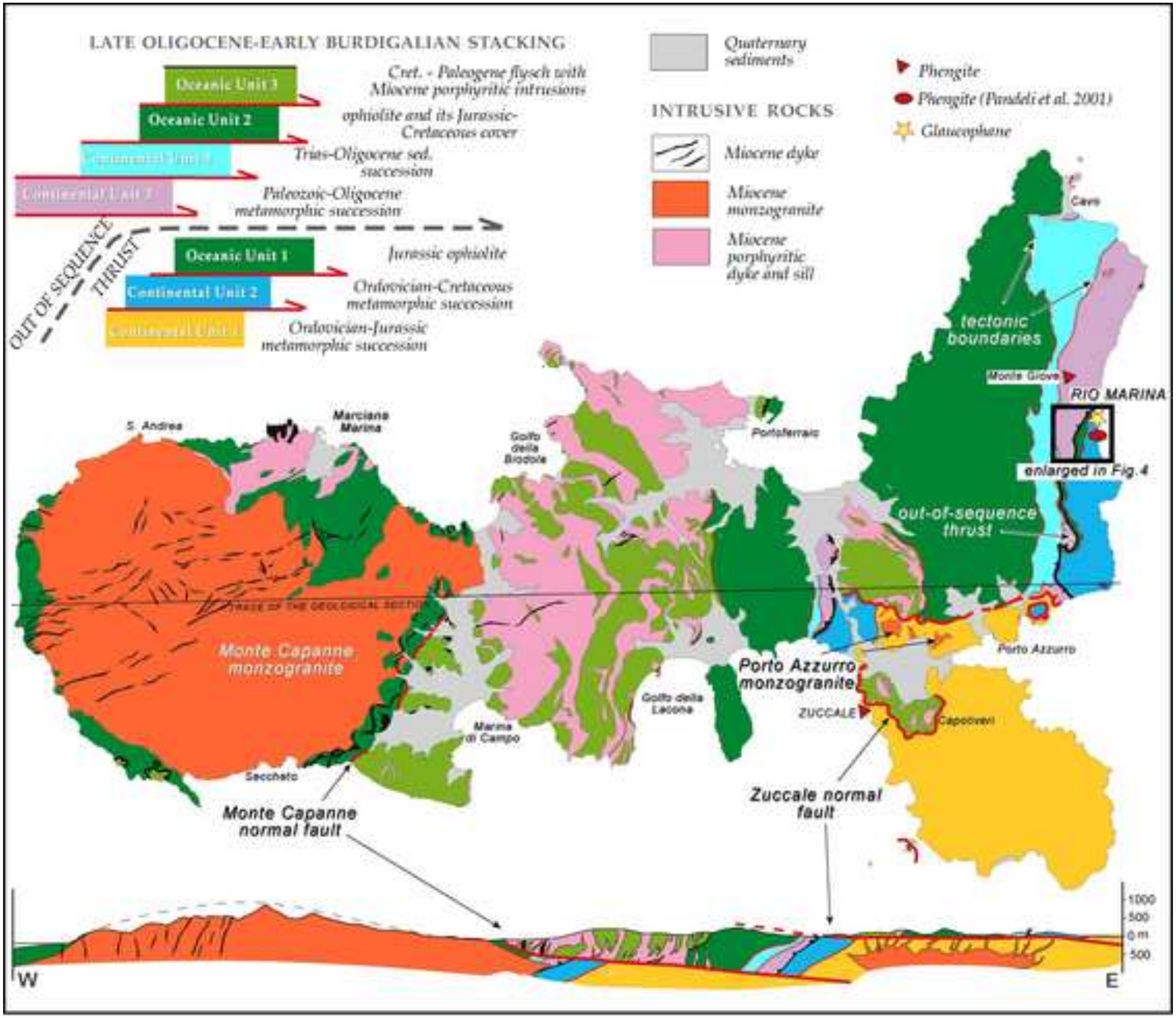

FIGURE 2

Figure3

Click here to download high resolution image

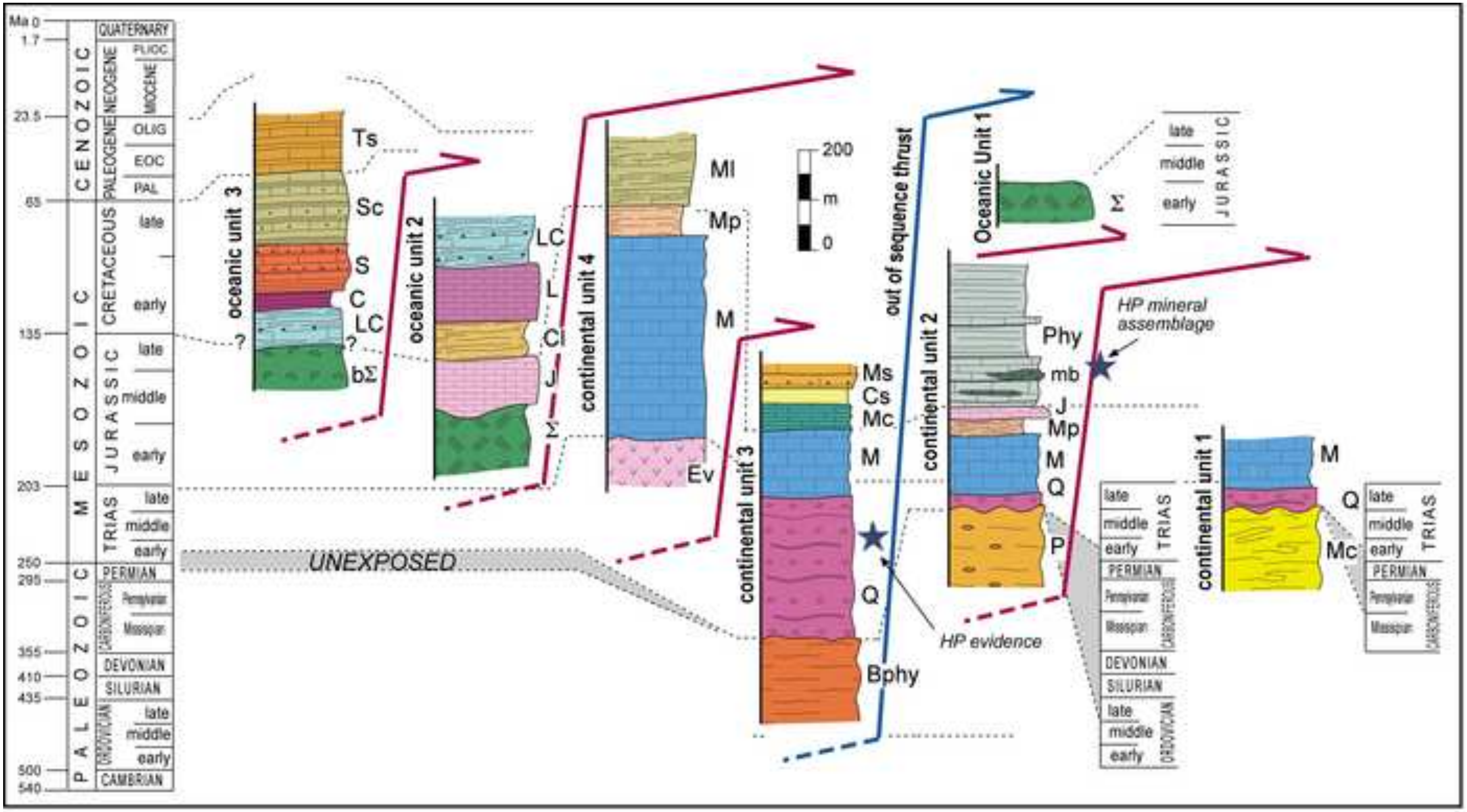

FIGURE 3

Figure4

Click here to download high resolution image

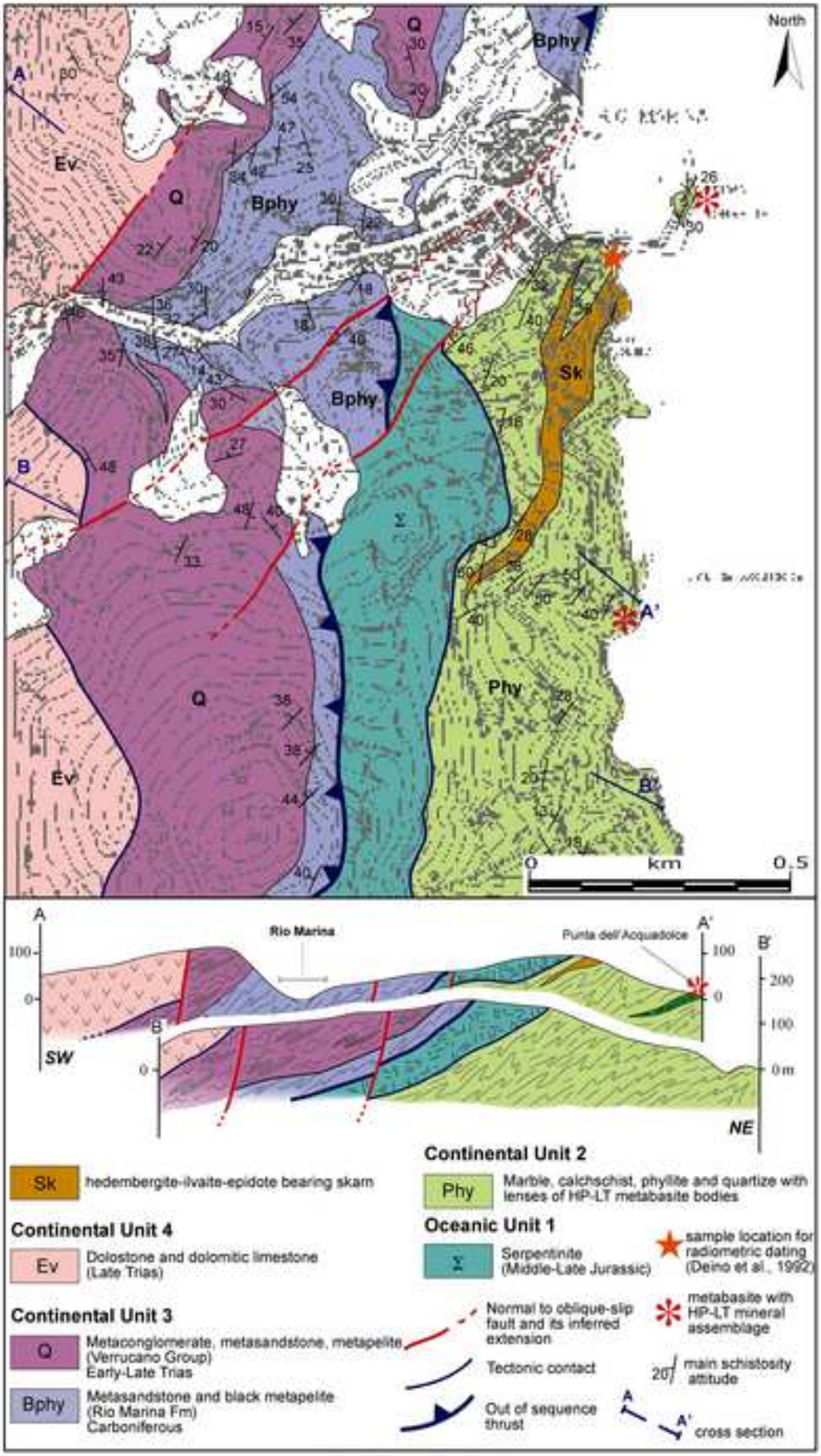

FIGURE 4

Figure5

Click here to download high resolution image

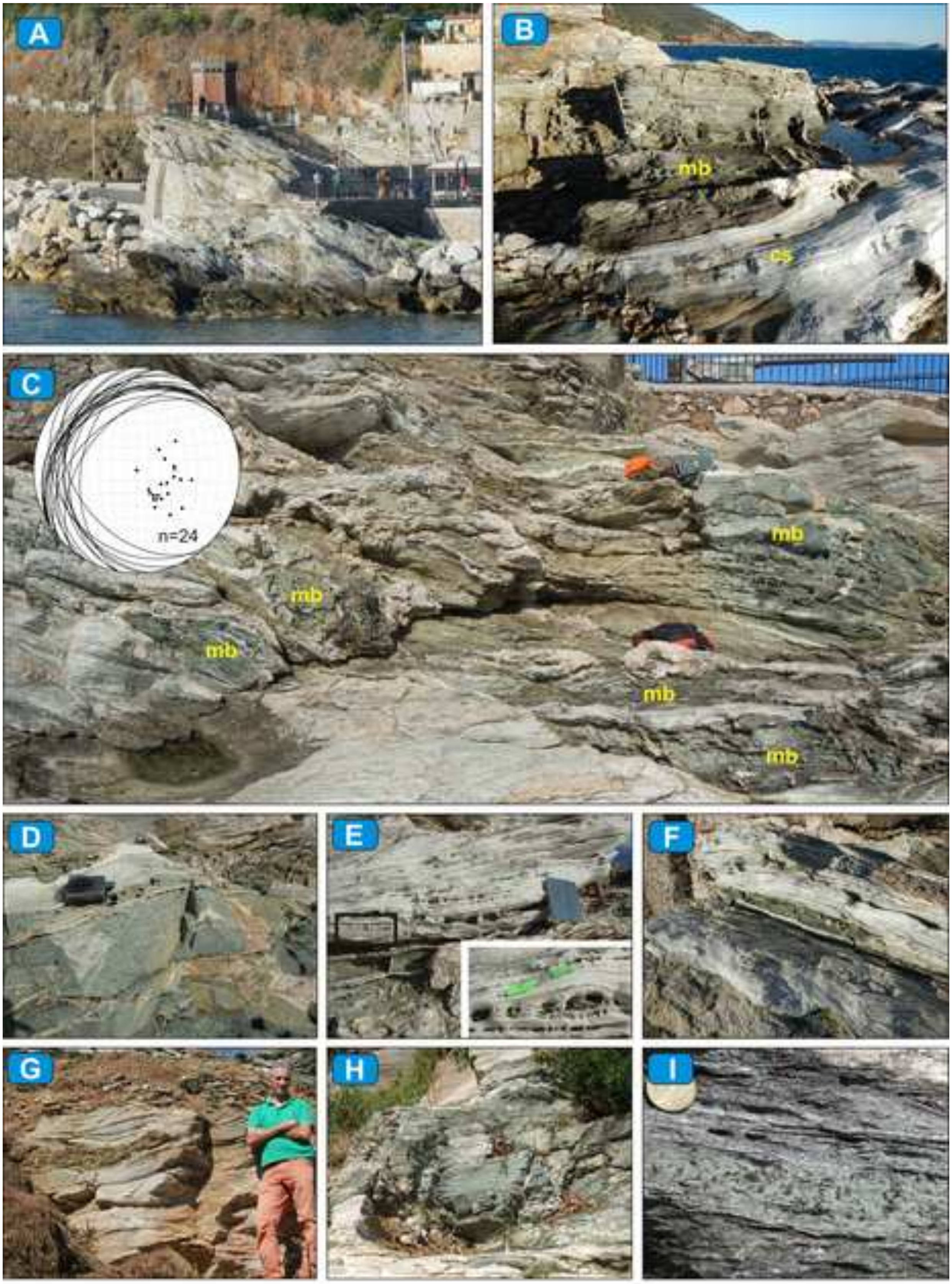

FIGURE 5

Figure6
Click here to download high resolution image

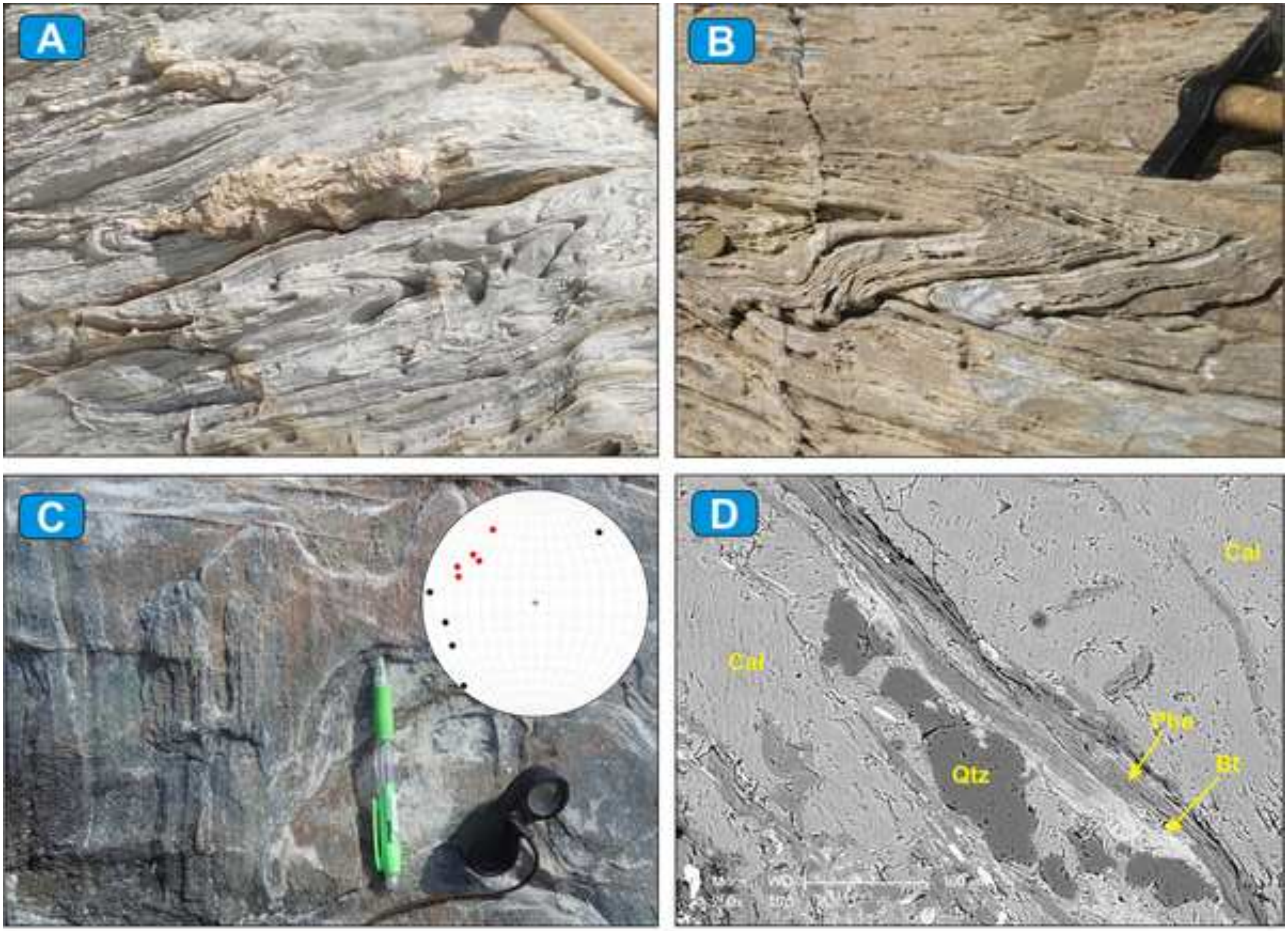

FIGURE 6

Figure7

Click here to download high resolution image

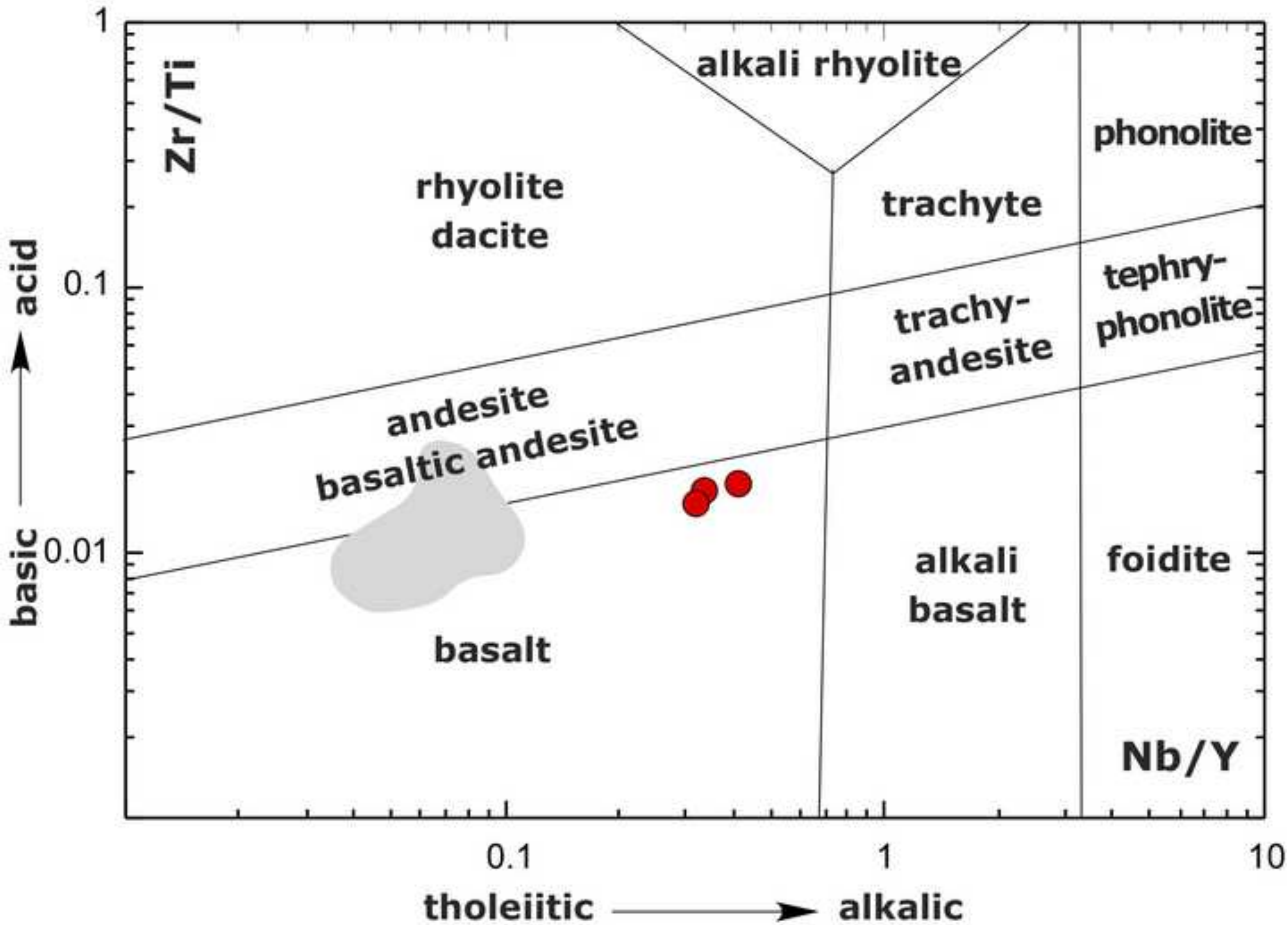

Figure8
Click here to download high resolution image

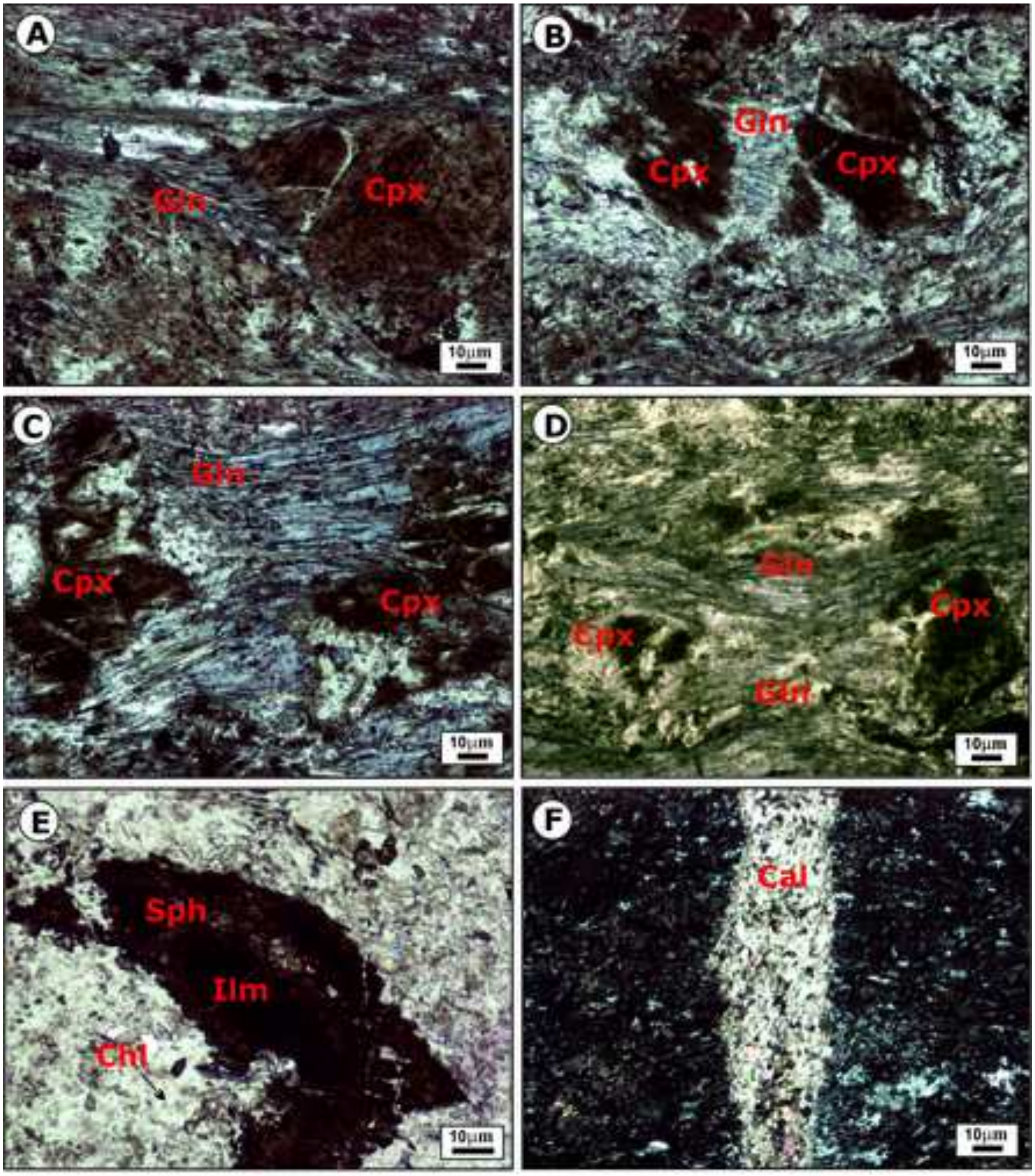

FIGURE 8

Figure9
Click here to download high resolution image

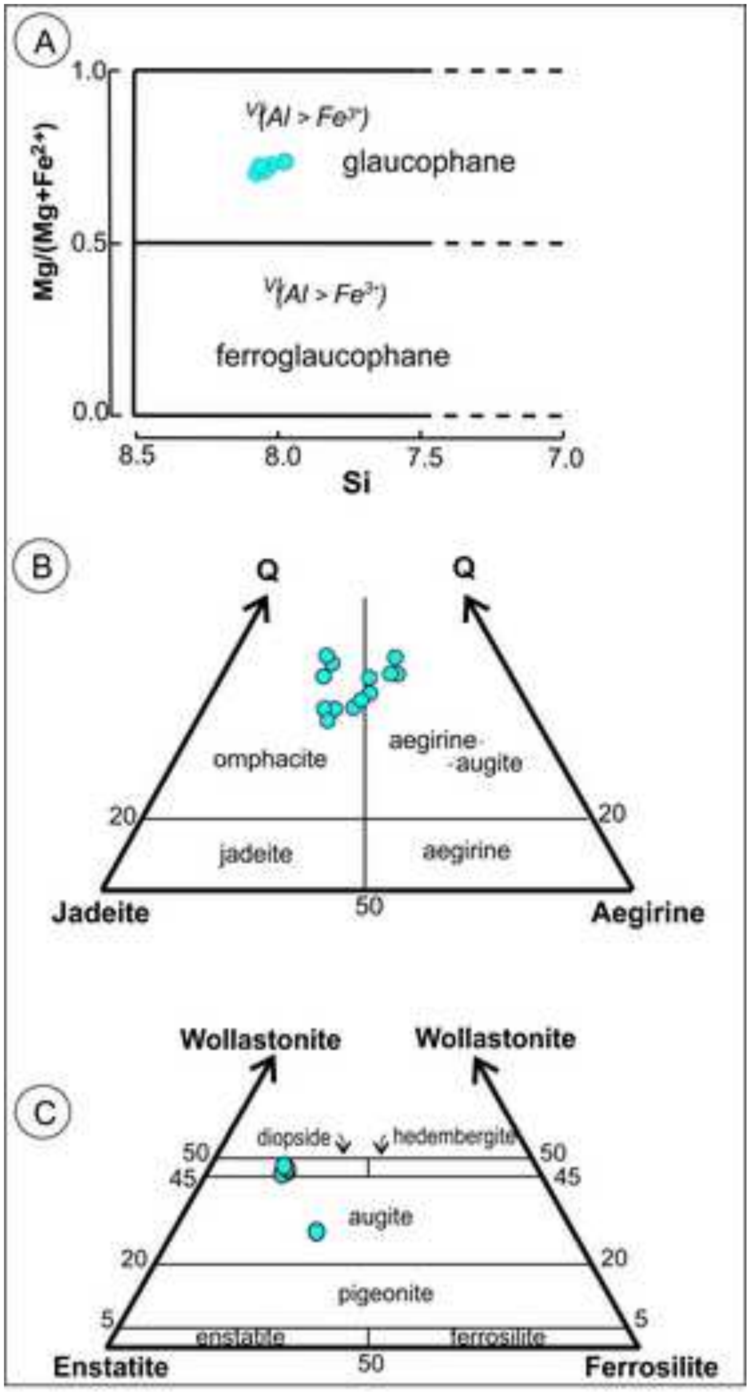

FIGURE 9

Figure10
Click here to download high resolution image

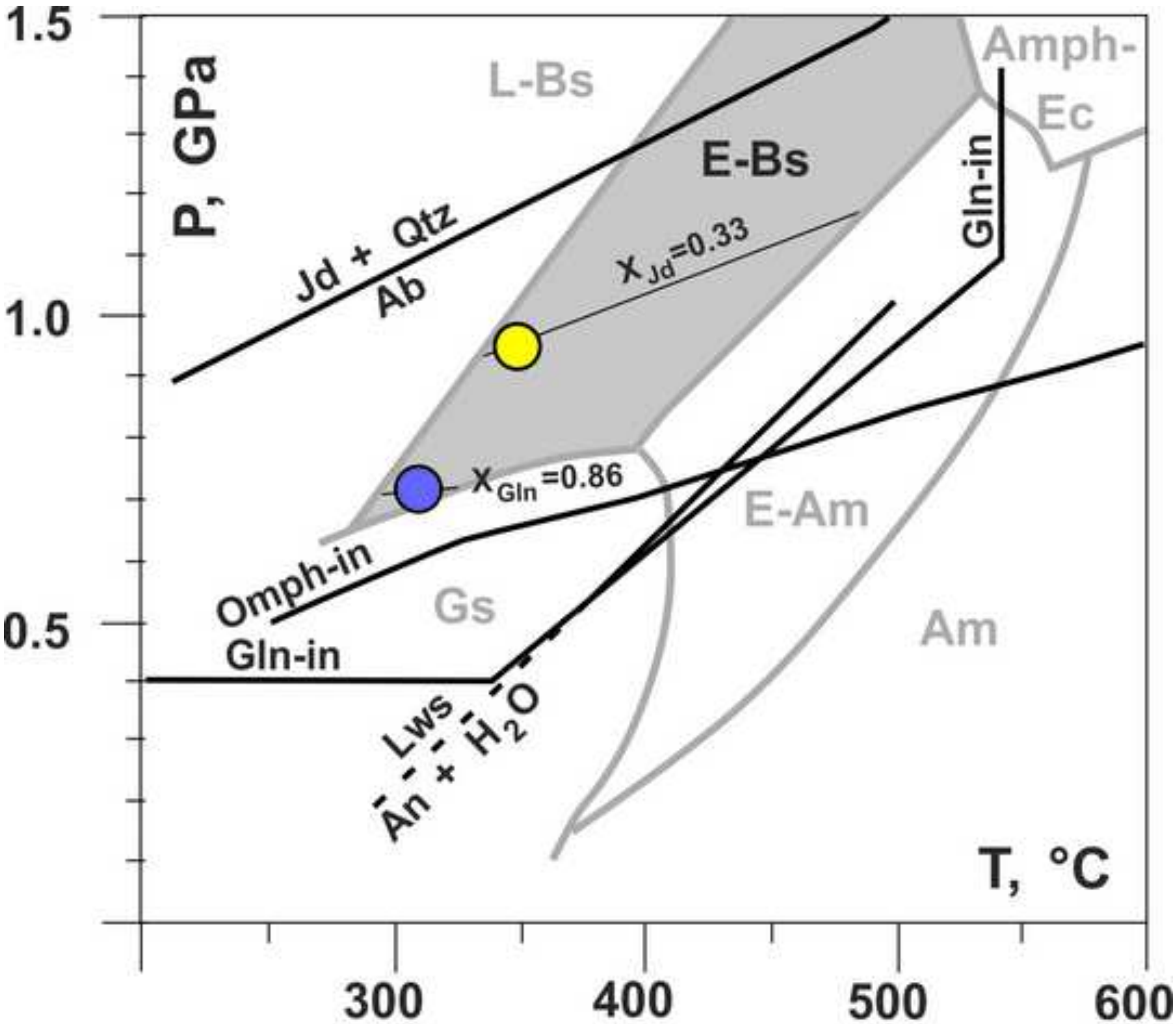

FIGURE 10

Figure11

Click here to download high resolution image

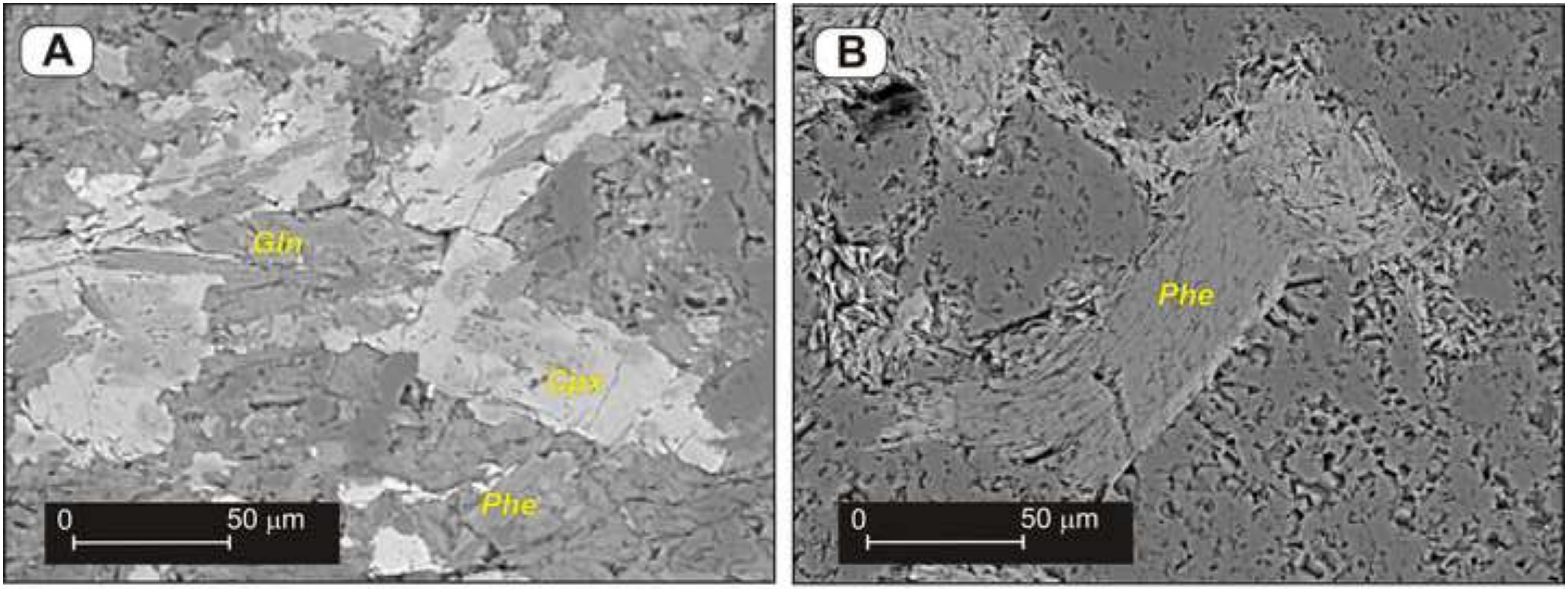

FIGURE 11